Inorganica Chimica Acta 586 (2025) 122785

Contents lists available at ScienceDirect

Inorganica Chimica Acta

journal homepage: www.elsevier.com/locate/ica

Novel zinc Metalloporphyrin based metal-organic framework for Quantitative & Reusable Sensing of nitrobenzene

Zachary Magnuson [a], Brielle Wolfe [a], Jacob M. Mayers [a,1], Lukasz Wojtas [a], Weijie Zhang [b,2], Shengqian Ma [b], Randy W. Larsen [a,*]

[a] Department of Chemistry, University of South Florida, Tampa, FL 33620, United States
[b] Department of Chemistry, North Texas State University, Denton, TX 76201, United States

ARTICLE INFO

Dataset link: ZnMMPF-X-NB (Original data)

Keywords:
Porphyrins
Photophysics
Metal-organic frameworks
Fluorescence
Sensing
Quenching
Turn-off
Metal Metalloporphyrin framework
Nitrobenzene
Nitroaromatics
Remediation
Detection
Quantitative
Stern-Volmer
Reusable sensor

ABSTRACT

Porphyrins and metalloporphyrins have been exploited for a wide range of applications including sensing and catalysis in both homogeneous and heterogeneous formats. An emerging class of porous materials that utilize porphyrins and metalloporphyrins for diverse applications are the metal organic frameworks (MOFs) containing porphyrins as guests within the MOF cavities or as integral components of the framework by serving as a metal node linker. Here, a novel metal metalloporphyrin framework (MMPF-X) was synthesized using a solvothermal method from a 4′,4‴,4⁗,4⁗′-(porphyrin-5,10,15,20-tetrayl)tetrakis(([1‴,1⁗-biphenyl]-3,5-dicarboxylic acid)) (TDBP) ligand and zinc paddlewheel metal building blocks (MBBs), yielding C 2/m space group crystals with a cph pattern of crisscross metalloporphyrin lattices that result in complex interconnected channels. The MMPF-X functions as a heterogeneous sensor for nitroaromatics, exhibiting reversible fluorescence quenching in the presence of nitrobenzene. The level of detection (LOD) was determined and compared to ZnTDBP in solution, highlighting MMPF-x's potential for quantitative sensing of nitrobenzene and related compounds across a wide concentration range. The quenching mechanism was evaluated using a modified stern-Volmer analysis for fractional components consistent with the porosity of the MOF.

1. Introduction

Porphyrins and metalloporphyrins exhibit diverse electronic properties leading to applications in optical based sensing, catalysis, and light harvesting [1,2]. With regards to chemical sensing, porphyrins have been utilized in a wide array of technologies including, but not limited to, functionalized polymers, thin films, porous materials, graphenes, and nanoparticles [3–6]. Although many porphyrinic chemical sensors are electrochemically based, their optical characteristics provide higher sensitivity [7,8].

Metal-organic frameworks (MOFs) are a class of materials that are important platforms for the incorporation of porphyrin-based sensor elements [9–12]. MOFs are composed of metal ion complexes known as metallo-building blocks (MBBs) that are linked together through organic ligands to form 2D and 3D porous framework structures. MOFs provide several advantages for small molecule sensing applications, including high surface area, tunable pore size, and chemical and thermal stability. The porosity of MOFs allows for small molecules to enter the pores and interact with the metal ions or organic linkers, which can result in changes in the electronic, optical, and/or magnetic properties of the MOF. Porphyrin metal-organic frameworks (PMOFs) are a subclass of MOFs that have demonstrated potential for sensing applications

Abbreviations: MOF, metal-organic framework; MMPF-X, metal metalloporphyrin framework; NB, nitrobenzene; MOF, PMOF, porphyrinic; SV, Stern-Volmer; SE, Stokes-Einstein; MBB, metal building block; LOD, level of detection.

* Corresponding author.
E-mail address: rwlarsen@usf.edu (R.W. Larsen).
[1] Current Adress: Johnson and Johnson Copr., Jaxsonville, Fl.
[2] Current Address: Department of Chemistry, University of Virginia. Charlottesville, VA.

https://doi.org/10.1016/j.ica.2025.122785
Received 27 March 2025; Received in revised form 22 May 2025; Accepted 23 May 2025
Available online 23 May 2025

[12–15]. PMOFs are constructed using porphyrins and metalloporphyrins as linkers between the framework MBBs [16–18]. Various PMOFs have displayed effective sensing of a wide range of small molecules, including nitroaromatics [19–21]. The sensing mechanism typically involves the interaction of the molecules with the porphyrin ligands in the MOF, which results in changes in the electronic and/or optical properties of the material.

One subclass of PMOFs are the MMPFs utilizing various octatopic and tetratopic porphyrin ligands that form a diverse array of MOF topologies [22–26]. The MMPFs containing open shell metals such as Co (II) or Pd(II) have been shown to be effective catalysts for numerous process including epoxidation reactions [24]. A particularly interesting material is MMPF-10 which contains a tetrakis-3,5-bis[(4-carboxy) phenyl]phenyl porphine (TBCPPP) ligand and Cu(II) within the porphyrin core. MMPF-10 catalyzes a reaction between CO_2 with aziridines to synthesize oxazolidinones [24,25]. The MMPF-9 MOF contains another octatopic ligand tetrakis(3,5-dicarboxybiphenyl)porphine which, in the presence of Cu(II) generates $Cu_2(CO_2)_4$ paddlewheel nodes with excellent performance as a heterogeneous Lewis-acid catalyst for chemical fixation of CO_2 to form carbonates at room temperature under 1 atm pressure [24,25].

In order to expand the functional versatility of the MMPFs, MMPF-X was prepared using the TDBP as a linker which forms paddle wheel nodes containing Zn(II) ions (Fig. 1). The emissive properties of MMPF-X present an opportunity for the development of both light-on and light-off sensors for a variety of analytes. The ability of MMPF-X to detect the model nitroaromatic compound nitrobenzene (NB) using a light-off mechanism has been explored using a modified Stern-Volmer mechanism [12].

2. Experimental

All reagents were purchased from Sigma-Aldrich, Fischer Scientific, and TCI America, and used without further purification unless otherwise noted.

Synthesis of TDBP and MMPF-X: TDBP was prepared using methods described in the SI. MMPF-X was prepared by a solvothermal method as follows: 4 mg of TDBP and 12 mg of $Zn(NO_3)_2{\cdot}6H_2O$ were added to 2 mL of DMSO in a 5-dram threaded cap glass vial and sonicated for ten minutes. The resulting solution was heated in a gravity oven at 135 °C for 72 h. The resulting red crystals were washed several times with DMSO and then soaked in MeOH for 24 h before being washed again with MeOH. Crystals were crushed in a mortar and pestle and then sonicated briefly in MeOH prior to use in all spectroscopy experiments.

Optical Absorption Spectroscopy: UV/Vis spectra were obtained from ~0.7 mg of a powdered MMPF-X suspension in 2 mL of methanol added to a 1-cm quartz optical cuvette, accompanied by stirring. Spectra were obtained on a Shimadzu UV2400 Spectrometer.

Steady-state Emission Spectroscopy: Steady state emission spectra were obtained using the same samples as for the UV/Vis spectroscopy. Emission spectra were obtained with an ISS PC1 single photon counting emission spectrometer with Soret excitation (426 nm for the TDBP and 430 nm for the MMPF-X).

Emission Lifetime Measurements: Samples were prepared as above and singlet lifetimes were determined using an ISS ChronosBH equipped with a Becker, Hinkl 473 nm pulsed laser diode operating at 20 MHz (~50 ps FWHM, ~0.6 mW), with a polarizer at the magic angle, and a 530 nm long-pass filter. A didodecyldimethylammonium bromide (DDAB) solution in H_2O was used as a reference to obtain the instrument response function. Data were fit using ISS Vinci software.

Reusability: Samples were prepared in the manner described above and kept under argon. Baseline fluorescence spectra were collected in the absence of NB, and subsequent spectra were obtained following the addition of 20 uL of neat NB immediately after the addition. The NB-containing MOF suspension was then centrifugated and decanted once, and argon-sparged MeOH was added to restore the original volume. This suspension was mixed thoroughly before being returned to the cuvette. The atmospheric headspace was replaced with argon and the sample was allowed to stir for 5 and 10 min before spectra was collected. This process was repeated once more before the quenched fluorescence intensity/lifetimes were returned to base line levels.

Single-Crystal X-Ray Crystallography: Single Crystals of MMPF-X and MMPF-Y were isolated directly from the supernatant solution and diffraction data were collected on a Bruker D8 VENTURE Single Crystal Diffractometer. The X-ray diffraction data for both crystals were collected using synchrotron radiation (λ = 0.41328 Å) at Advanced Photon Source, Beamline 15-ID-B of ChemMatCARS in Argonne National Lab, Argonne, IL Indexing was performed using APEX326. Data integration and reduction was performed using SaintPlus [27]. Absorption correction was performed by a multi-scan method implemented in SADABS [28]. Space groups were determined using XPREP implemented in APEX3. Structures were solved using SHELXT [29] and refined using SHELXL-2019 (full-matrix least-squares on F2) through Olex2 [30].

3. Results and discussion

3.1. Structural Characterization of MMPF-X

The MMPF-X framework is disordered about symmetry positions and was refined using restraints. Due to the disorder, the assignment and the exact number of solvent molecules is tentative. The framework appears to be negatively charged, but it was not possible to identify the counterions. The contribution of heavily disordered content in the structural voids was treated as diffuse using the Squeeze procedure implemented in the Platon program [31]. Crystal data and refinement conditions are listed in Tables S1 and S2 in the SI. The crystals diffracted only up to ca. 1.3 Å resolution. Disordered ligands were modeled with restraints. Due

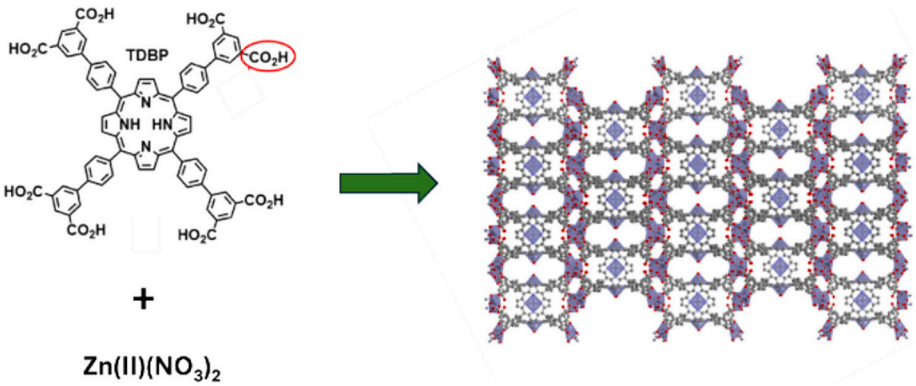

Fig. 1. Schematic illustration of TDBP + Zn paddlewheel combined to produce MMPF-X.

to the high symmetry and disorder, it was not possible to locate anions or solvent molecules.

The MMPF-X structure consists of infinite ribbons made of Zn / carboxylate clusters (Fig. 1 and Fig. 2) bridged by two types of crystallographically independent and tetragonally shaped porphyrin ligands. The resulting 3-D framework contains structural channels along the crystallographic [001]/c direction filled with heavily disordered content and providing access to the porphyrin active sides in the crystal. The total available free space after removal of solvent molecules is approximately 75 %.

3.2. Spectroscopic Characterization of Zn TDBP and MMPF-X

The absorption and emission spectra of the parent Zn TDBP ligand are displayed in Fig. 3, left panel. The absorption spectrum of the ZnTDBP in methanol is dominated by a Soret band (B(0,0)) centered at 426 nm that originates from the porphyrin π to π* transition and attributed to mixtures of a_{1u} - > e_g and a_{2u} - > e_g orbital excitations in Gouternman's classical four orbital model [32]. The corresponding visible bands are attributed to the Q(0,0) (557 nm) and Q(0,1) (600 nm) transitions. The absorption bands of the Zn TDBP are bathochromically shifted by ~6 nm from the parent Zn(II) tetraphenyl porphyrin (ZnTPP) (B(0,0) ~420 nm, Q(0,0) ~550 nm and Q(0,1) ~594 nm) indicating the extension of the peripheral phenyl groups couple to the porphyrin ring. The ZnTDBP emission spectrum exhibits two bands corresponding to decay of the Q(0,0) and Q(0,1) excited states (S_1 state) (605 nm and 655 nm, respectively). The emission maxima are independent of the excitation wavelength, again, consistent with emission arising from decay of the S_1 state.

The absorption spectrum of the MMPF-X framework suspension in methanol displays a Soret band at 430 nm and Q-bands at 552 nm and 610 nm. The corresponding emission bands are observed at 623 nm and 664 nm (also independent of excitation wavelength). The fact that the absorption bands of the MMPF-X and ZnTDBP are similar indicates that there are no significant structural perturbations associated with incorporation of the macrocycle into the framework that affect the energy of the excited S_2 state. However, the longer wavelengths associated with the emission bands of the MMPF-X indicated perturbations that lower the energy of the emitting S_1 state and a relative increase in decay to a vibrational mode of the ground state.

3.3. Emission Quenching of ZnTDBP by Nitrobenzene

The quenching of the ZnTDBP by NB is displayed in Fig. 4. Both the Q (0,0) and Q(0,1) bands decrease in intensity upon addition of NB (Fig. 4, left panel) with a corresponding decrease in lifetime (Fig. 4, right panel). An overlay of the Stern-Volmer plots derived from the emission lifetimes and emission intensities are displayed in Fig. 5.

The (I_0/I) Stern-Volmer (SV) plot for the ZnTDBP quenching is linear and characteristic of a diffusional quenching process that can be described by the classic Stern-Volmer equation:

$$\frac{I_0}{I} = 1 + k_q \tau_o [Q] \quad (1)$$

where I_0 is the fluorescence intensity in the absence of quencher, I is the fluorescence intensity at various [Q], kq is the quenching rate constant (M^{-1} s^{-1}), and τ_0 is the fluorophore lifetime in the absence of quencher (6.1 ns for ZnTDBP, Fig. 5, left panel) [33]. From the SV analysis, ZnTDBP exhibits a dynamic quenching mechanism with a $k_q = 5 \times 10^9$ M^{-1} s^{-1}. The k_q value is similar to other Zn(II) porphyrins including Zn (II) tetrasulphonatophenyl porphyrin (ZnTPPS) ($k_q = 4 \times 10^{10}$ M^{-1} s^{-1}) [34–36]. The quenching mechanism involves photo-induced electron transfer between the excited state porphyrin and NB within a solvent excluded contact pair according to:

ZnP* + NB - > [ZnP^+:NB^-] - > ZnP + NB Scheme 1 [37].

3.4. MMPF-X NB emission quenching

The corresponding steady state emission quenching of the MMPF-X MOF in the presence of NB is non-linear with two concentration ranges (Fig. 5, right panel). The non-linear SV plot can be attributed to more than one type of quenching interaction between NB and fluorophore consistent with the porous structure of the MOF [38]. Emission quenching associated with several photo-active MOFs has been shown to be diffusion controlled, with diffusion rates dependent on guest size with respect to MOF channel and pore sizes [39–41]. In contrast, the τ_0/τ plot is indicative of a pure static mechanism (τ_0 is 1.3 ns for MMPF-X).

The SV data can be best interpreted using an SV equation that is modified to account for fractional contribution of multiple components, in which the populations have different accessibility to the quencher:

$$\frac{I_0}{I} = \sum_{i=1}^{n} \frac{f_i}{(1 + k_{qi}\tau_0[Q])} \quad (2)$$

where f_i is the fraction of fluorophores with associated quenching rate constant k_{qi} [38]. Fitting the steady state SV data to Eq. 2 results in two fractional populations of accessible quenching sites, one that is static in character with $f_1 = 0.47 \pm 0.02$ and $k_{SV1} = 0$, and a second that is dynamic in character with $f_2 = 0.53 \pm 0.02$, and a $k_{SV2} = 10.9 \times 10^4$ M^{-1}. The fraction of accessible sites making up 53 % of the total population are proposed to be ZnTDBP sites located on the surface of the crystal that are quenched through diffusional interactions with the solution NB. The corresponding fraction accounting for the remaining 47 % of the sites are proposed to be interior framework ZnTDBP ligands that are quenched by NB molecules that populate the interior cavities of the MOF.

Fig. 6 illustrates the quenching model for the MMPF-X. The population of chromophores giving rise to the diffusional quenching are primarily surface accessible sites. Upon addition of NB to MMPF-X, NB molecules colliding with the crystal surface porphyrins give rise to the diffusional quenching process while NB that encounter an aperture enter the MOF cavities and statically quench interior porphyrins associated with the framework cavities. As the concentration of NB increases the population of NB occupied cavities resulting in increased static quenching.

3.5. Diffusional quenching efficiency

The Stokes-Einstein (SE) relation describes an approximation of the rate at which diffusion-limited bimolecular collisions can occur in a solution of known viscosity, k_d.

$$k_d = \frac{8RT}{3\eta} \quad (3)$$

where R is the gas constant, T is temperature, and η is the viscosity of the medium [38]. In MeOH at standard temperature and pressure, k_d =

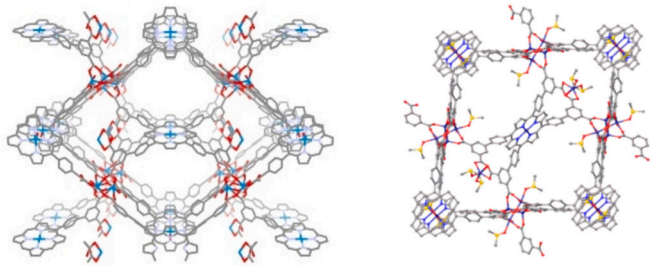

Fig. 2. Crystal structure of MMPF-X. Atom by colour: Gray (carbon), red (oxygen), lavender (nitrogen), and light blue (zinc). Hydrogen not displayed for clarity. (For interpretation of the references to colour in this figure legend, the reader is referred to the web version of this article.)

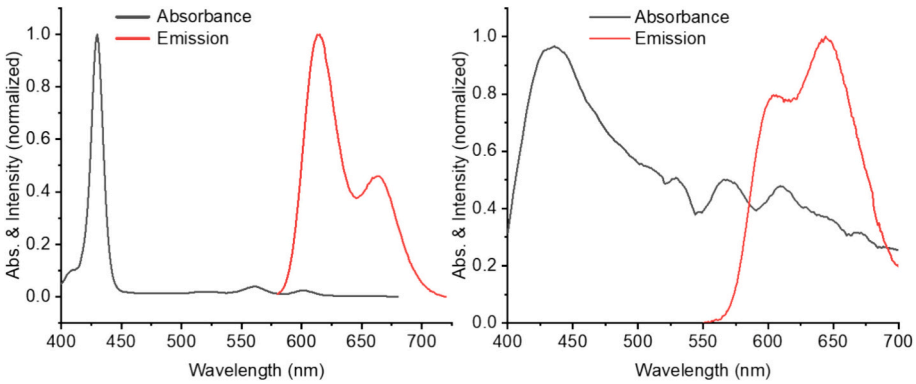

Fig. 3. Normalized UV–Vis absorbance and fluorescence emission spectra for ZnTDBP (left) and MMPF-X (right) in methanol.

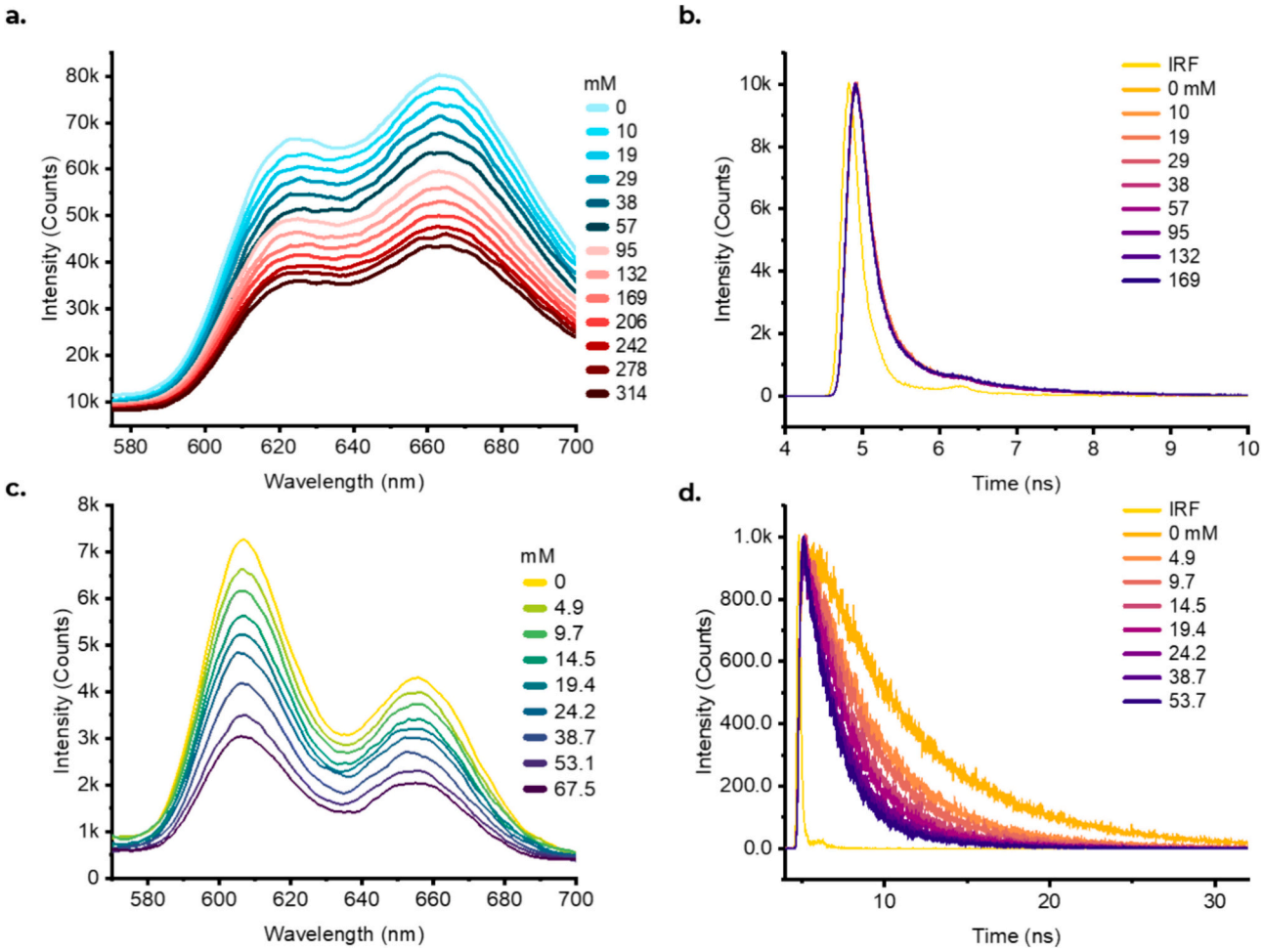

Fig. 4. a, b. Change in fluorescence emission intensity and lifetime of ZnTDBP upon the addition of NB. c, d. Change in fluorescence emission intensity and lifetime of MMPF-X upon the addition of NB.

1.24×10^{10} M^{-1} s^{-1}, which can be compared to the ligand and MOF quenching constants to estimate the efficiency of diffusional quenching (bimolecular collision of NB with fluorophore) relative to an ideal solution. When compared as a percentage ($k_{qi}*k_d^{-1}*100$ %), the quenching rate for the diffusional component of MMPF-X (69 %) is nearly the same as ZnTDBP in solution (65 %) at the same total concentration of fluorophore.

This comparison indicates there is little difference between the availability of homogeneous ZnTDBP and the surface accessible ZnTDBP in the heterogeneous MMPF-X suspension. This also highlights the inefficiency inherent to homogeneous porphyrins, which are known to form deactivated stacking dimers and oligomers [21].

3.6. *Recycling and sensitivity*

The sensitivity of MMPF-X towards the quantitative detection of NB was determined by the limit of detection (LOD) for both the MOF and the metalloporphyrin in solution. The LODs were obtained using Stern-

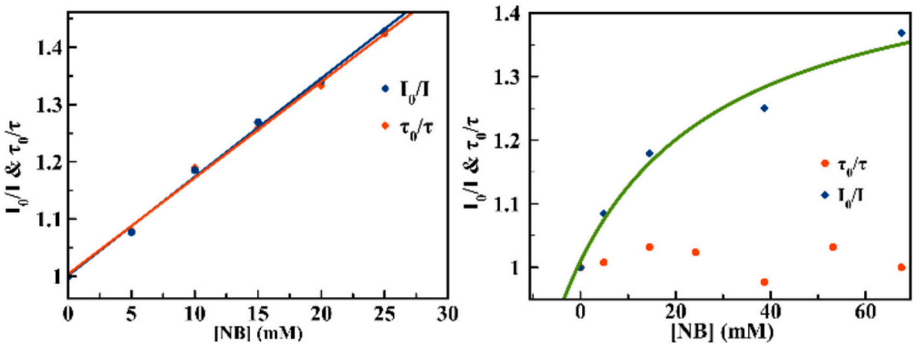

Fig. 5. Plot of I_0/I and τ_0/τ associated with Zn TDBP (left) and MMPF-X (right) upon the addition of NB.

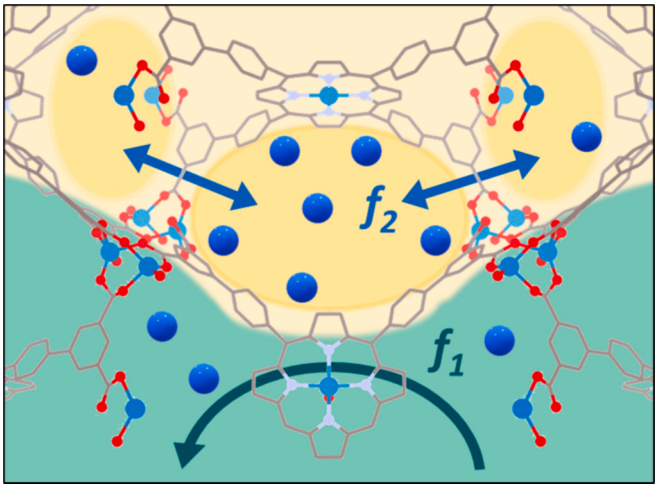

Fig. 6. Illustration of nitrobenzene quenching by MMPF-X. The yellow highlighted area and blue arrows represent the MOF interior and quenching by NB within, as well as NB diffusion between pores, accounting for component f_2. The green arrow represents collisional quenching at the exterior, where bulk solution is highlighted light green. (For interpretation of the references to colour in this figure legend, the reader is referred to the web version of this article.)

Volmer analysis. ZnTDBP exhibits a LOD of 1.5 mM, while MMPF-X exhibits LOD of 2.6 mM. While ZnTDBP has overall lower thresholds of detection for quantitative measurement, MMPF-X is sensitized towards a significantly broader range of concentrations of NB, with a relatively smaller increase in its detection limitations. Relative to other heterogeneous materials MMPF-X performs similarly in the detection of NB (Table 1).

4. Conclusion

The ability to recycle MMPF-X as a nitro sensor is augmented by the facile separation inherent in heterogeneous materials. Fig. 7 demonstrates that the initial fluorescence intensity of MMPF-X can be regenerated by filtering the powdered solid and washing with MeOH several times; NB is easily removed from the MOF, indicating reversible

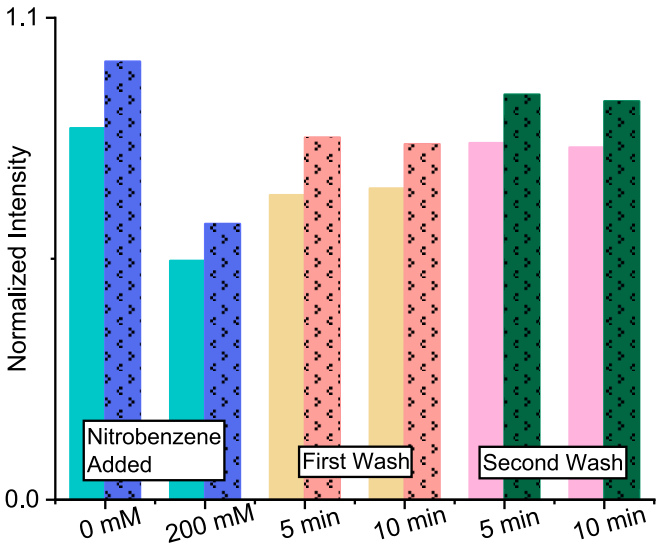

Fig. 7. Normalized emission spectra of MMPF-X illustrating regeneration of emission intensity after addition and subsequent washing with methanol. Solid and patterned bars represent fluorescence emission maxima at 623 and 664 nm, respectively.

Table 1
Comparison of K_{SV} values of several MOF-based nitroaromatic sensors. These materials all utilize fluorescence emission quenching for detection. Acronyms: NP (nitrophenol), NA (nitroaniline).

Material	Sensor	Analyte	Ksv (M^{-1})	Solvent	Refs.
$[Pb_{1.5}(DBPT)]_2{\cdot}(DMA)_3(H_2O)_4$	DBPT	NB	1.4×10^4	Water	[40]
FJI-C8	H_6TDPAT	2,4-DNP	5.1×10^4	DMF	[41]
ZSTU-2	H_3BTB	Picric Acid	2.3×10^4	EtOH	[42]
–	–	NB	1.4×10^4	–	
HNU-34	H_4TCPE	TNP	3.1×10^4	DMF	[43]
–	–	3-NP	86	–	
$[Cd(L){\bullet}H_2O]_n$	$[Cd(L){\bullet}H_2O]_n$	TNP	1.6×10^4	Water	[44]
–	–	4-NP	5.2×10^3	–	
$[Cd_3(DBPT)_2(H_2O)_4]{\cdot}5H_2O$	H_3DBPT	TNP	2.8×10^4	MeOH	[45]
–	–	4-NA	2.5×10^4	–	
CdHTBA	NTBA	NB	0.3×10^4	EtOH	[46]
Zn2 -(NDC)2 (bpy)·Gx	Zn-NDC	NB	4.6×10^4	EtOH	[47]
MMPF-X	Zn TDBP	NB	1.1×10^4	MeOH	*this work*
ZnTDBP	Zn TDBP	NB	2.9×10^4	MeOH	*this work*

interaction between MMPF-X and NB. The application of novel MMPF-X as a reusable, heterogeneous optical sensor of model compound nitrobenzene, functioning across a wide concentration range, makes it suitable for applications that require facile and rapid detection. Future work in the application of this system would benefit from selectivity studies, such as the detection of NB against concomitants such as those speciated in real-world samples or functionally similar chemicals.

CRediT authorship contribution statement

Zachary Magnuson: Writing – original draft, Visualization, Methodology, Investigation, Formal analysis, Conceptualization. **Brielle Wolfe:** Investigation. **Jacob M. Mayers:** Writing – review & editing, Methodology, Investigation, Formal analysis. **Lukasz Wojtas:** Writing – original draft, Formal analysis. **Weijie Zhang:** Methodology, Investigation, Formal analysis. **Shengqian Ma:** Supervision, Project administration, Methodology, Investigation, Formal analysis. **Randy W. Larsen:** Writing – review & editing, Writing – original draft, Supervision, Project administration, Methodology, Investigation, Formal analysis.

Funding sources

USF College of Arts and Sciences Research Funds (RWL).

Declaration of competing interest

The authors declare that they have no known competing financial interests or personal relationships that could have appeared to influence the work reported in this paper.

Acknowledgment

The Authors would like to acknowledge the College of Arts and Sciences, Office of Research and Scholarship for support of this work.

Appendix A. Supplementary data

Supplementary data to this article can be found online at https://doi.org/10.1016/j.ica.2025.122785.

Data availability

Data will be made available on request.
ZnMMPF-X-NB (Original data) (USF Digital Commons)

References

[1] Y. Ding, W.-H. Zhu, Y. Xie, Development of ion chemosensors based on porphyrin analogues, Chem. Rev. 117 (4) (2017) 2203–2256.
[2] J.C. Barona-Castaño, C.C. Carmona-Vargas, T.J. Brocksom, K.T. De Oliveira, Porphyrins as catalysts in scalable organic reactions, Molecules 21 (3) (2016) 310.
[3] N.U. Day, C.C. Wamser, M.G. Walter, Porphyrin polymers and organic frameworks, Polym. Int. 64 (7) (2015) 833–857.
[4] L. Smykalla, C. Mende, M. Fronk, P.F. Siles, M. Hietschold, G. Salvan, D.R. Zahn, O. G. Schmidt, T. Rüffer, H. Lang, (Metallo) porphyrins for potential materials science applications, Beilstein J. Nanotechnol. 8 (1) (2017) 1786–1800.
[5] Z.-L. Qi, Y.-H. Cheng, Z. Xu, M.-L. Chen, Recent advances in porphyrin-based materials for metal ions detection, Int. J. Mol. Sci. 21 (16) (2020) 5839.
[6] Y. Zhou, X. Liang, Z. Dai, Porphyrin-loaded nanoparticles for cancer theranostics, Nanoscale 8 (25) (2016) 12394–12405.
[7] C. Di Natale, D. Monti, R. Paolesse, Chemical sensitivity of porphyrin assemblies, Mater. Today 13 (7–8) (2010) 46–52.
[8] X. Zhang, M.C. Wasson, M. Shayan, E.K. Berdichevsky, J. Ricardo-Noordberg, Z. Singh, E.K. Papazyan, A.J. Castro, P. Marino, Z. Ajoyan, A historical perspective on porphyrin-based metal–organic frameworks and their applications, Coord. Chem. Rev. 429 (2021) 213615.
[9] Y. Li, G. Wen, J. Li, Q. Li, H. Zhang, B. Tao, J. Zhang, Synthesis and shaping of a metal organic frameworks: a review, Chem. Commun. 58 (2022) 11488.
[10] F.V. Yusuf, N.I. Malek, S.K. Kailasa, Review on metal organic framework classification, synthetic approaches, and influencing factors: applications in energy, drug discovery, and wastewater treatment, ACS Omega 7 (2022) 44507–44531.
[11] Y. Cheng, S.J. Datta, S. Zhou, J. Jia, O. Shekha, M. Eddaoudi, Advances in metal organic framework-based membranes, Chem. Soc. Rev. 51 (2022) 8300.
[12] J.A. Martin-Illan, D. Rodriguez-San-Miguel, F. Zamora, Evolution of covalent organic frameworks: from design to real-world applications, Coord. Chem. Rev. 495 (2023) 215342.
[13] L.E. Kreno, K. Leong, O.K. Farha, M. Allendorf, R.P. Van Duyne, J.T. Hupp, Metal organic framework materials as chemical sensors, Chem. Rev. 112 (2012) 1105–1125.
[14] D. An, L. Chen, Y. Liang, J. Hou, J. Chen, Defect containing metal organic framework materials for sensor applications, J. Mat. Chem. A 12 (2024) 38.
[15] J. Qin, J. Li, H. Zeng, J. Tang, D. Tang, Recent advances in metal organic framework based photoelectrochemical and electrochemiluminescence biosensors, Analyst 148 (2023) 2200.
[16] C. Tang, X. Li, Y. Hu, X. Du, S. Wang, B. Chen, S. Wang, Porphyrin-based metal organic framework materials: design, construction, and applications in the field of Photocatalysis, Molecules 29 (2024) 467.
[17] S.M. Sajjadinezhad, L. Boivin, K. Bouarab, P.D. Harvey, Photophysical properties and photonic applications of porphyrin based MOFs, Coord. Chem. Rev. 510 (2024) 215794.
[18] S. De, T. Devic, A. Fateeva, Porphyrinic and phthalocyanine-based metal organic frameworks beyond metal-carboxylates, Dalton Trans. 50 (2021) 1166.
[19] J. Yang, Z. Wang, K. Hu, Y. Li, J. Feng, J. Shi, J. Gu, Rapid and specific aqueous-phase detection of nitroaromatic explosives with inherent porphyrin recognition sites in metal–organic frameworks, ACS Appl. Mater. Interfaces 7 (22) (2015) 11956–11964.
[20] R. Dhir, M. Kaur, A.K. Malik, Porphyrin metal-organic framework sensors for chemical and biological sensing, J. Fluoresc. (2024), https://doi.org/10.1007/s10895-024-03674-0.
[21] T. Burger, M.V. Hernandez, C. Carbonell, J. Rattenberger, H. Wiltsche, P. Falcaro, C. Slugovc, S.M. Borisov, Luminescent Porphyrinic metal-organic frameworks for oxygen sensing: correlation of nanostructure and sensitivity, ACS Appl. Nano. Mat. 6 (2023) 248–260.
[22] W. Zhang, A. Nafady, C. Shan, L. Wojtas, Y.-S. Chen, Q. Cheng, X.P. Zhang, S. Ma, Functional Porphyrinic metal Oganic framework as a new class of heterogeneous halogen-bond-donor catalyst, Angew. Chem. Int. Ed. 60 (2021) 24312–24317.
[23] Z.L. Magnuson, Q. Cheng, W. Zhang, Y.-S. Chen, L. Wojtas, A. Nafady, A.M. Al-Enizi, R.W. Larsen, X.P. Zhang, S. Ma, Two Manganese Metalloporphyrin Frameworks Constructed from a Custom-Designed Porphyrin Ligand Exhibiting Selective Uptake of CO_2 over CH_4 and Catalytic Activity for CO_2 Fixation, Cryst. Growth Des. 21 (2021) 2786–2792.
[24] W.-Y. Gao, L. Wojtas, S. Ma, A porous metal–metalloporphyrin framework featuring high-density active sites for chemical fixation of CO_2 under ambient conditions, Chem. Commun. 50 (2014) 5316–5318.
[25] X.-S. Wang, M. Chrzanowski, L. Wojtas, Y.-S. Chen, S. Ma, Formation of a Metalloporphyrin-Based Nanoreactor by Postsynthetic Metal–Ion Exchange of a Polyhedral-Cage Containing a Metal–Metalloporphyrin Framework, Chem. Eur. J. 19 (2013) 3297–3301.
[26] Bruker, APEX3 Bruker AXS Inc., Madison, Wisconsin, USA, 2019.
[27] Bruker, SAINT V8.35A. Data Reduction Software, 2019.
[28] G.M. Sheldrick, SADABS. Program for Empirical Absorption Correction, University of Gottingen, Germany, 1996.
[29] XT, G.M., Sheldrick, Acta Crystallogr. A71 (2015) 3–8.
[30] O.V. Dolomanov, L.J. Bourhis, R.J. Gildea, J.A.K. Howard, H. Puschmann, OLEX2: a complete structure solution, refinement and analysis program, J. Appl. Crystallogr. 42 (2009) 339–341.
[31] A.L. Spek, Structure validation in chemical crystallography, Acta Crystallogr. D65 (2009) 148–155.
[32] M. Gouterman, G.H. Wagnière, L.C. Snyder, Spectra of porphyrins: part II, Four orbital model. J. of Mol. Spect. 11 (1–6) (1963) 108–127.
[33] M.H. Gehlen, The centenary of the stern-Volmer equation of fluorescence quenching: from the single line plot to the SV quenching map, J Photochem Photobiol C: Photochem Rev 42 (2020) 100338.
[34] M.S. Meaney, V.L. McGuffin, Investigation of common fluorophores for the detection of nitrated explosives by fluorescence quenching, Anal. Chim. Acta 610 (2008) 57–67.
[35] A. Rana, P.K. Panda, Fluorescent turn-off based sensing of nitrated explosives using porphyrins and their Zn (II)-derivatives, RSC Adv. 2 (32) (2012) 12164–12168.
[36] M. Takezaki, T. Tminaga, Fluorescence quenching reaction of porphyrins in micelles: ionic porphyrins quenched by nitrobenzene in ionic micelles, J. Photochem. Photobiol. A Chem. 174 (2005) 113–118.
[37] G.S. Nahor, J. Rabani, Charge separation and Photoreduction of zinc Tetrakis (sulfonatophenyl)porphyrin by nitrobenzene and Methylviologen in aqueous solution, J. Phys. Chem. 89 (1985) 2468–2472.
[38] J. Keizer, Nonlinear fluorescence quenching and the origin of positive curvature in stern-Volmer plots, J. Am. Chem. Soc. 105 (6) (1983) 1494–1498.
[39] A. Sharma, D. Kim, J.-H. Park, S. Rakshit, J. Seong, G.H. Jeong, O.-H. Kwon, M. S. Lah, Mechanistic insight into the sensing of nitroaromatic compounds by metal-organic frameworks, Comm. Chem. 2 (1) (2019) 39.
[40] Y. Sun, B.-X. Dong, W.-L. Liu, An adjustable dual-emission fluorescent metal-organic framework: effective detection of multiple metal ions, nitro-based molecules and DMA, Spect. Chim. Acta A: Mol. Biomol. Spect. 223 (2019) 117283.

[41] X.-S. Wang, L. Li, D.-Q. Yuan, Y.-B. Huang, R. Cao, Fast, highly selective and sensitive anionic metal-organic framework with nitrogen-rich sites fluorescent chemosensor for nitro explosives detection, J. Hazard. Mater. 344 (2018) 283–290.
[42] X. Zhang, Y. Yan, F. Chen, G. Bai, H. Xu, S. Xu, A fluorescent titanium-based metal-organic framework sensor for nitro-aromatics detection, Z. Anorg. Allg. Chem. 647 (7) (2021) 759–763.
[43] X. Zhang, G. Ren, M. Li, W. Yang, Q. Pan, Selective Detection of Aromatic Nitrophenols by a Metal–Organic Framework-Based Fluorescent Sensor, Cryst. Growth Des. 19 (11) (2019) 6308–6314.
[44] J. Zhang, J. Hu, C. Sun, X. Li, A thermal and pH stable fluorescent metal-organic framework sensor for high selectively and sensitively sensing nitro aromatic compounds in aqueous media, J. Mol. Struct. 1245 (2021) 131059.
[45] B.-X. Dong, Y.-M. Pan, W.-L. Liu, Y.-L. Teng, An Ultrastable Luminescent Metal–Organic Framework for Selective Sensing of Nitroaromatic Compounds and Nitroimidazole-Based Drug Molecules, Cryst. Growth Des. 18 (1) (2018) 431–440.
[46] A.-X. Zhu, Z.-Z. Qiu, L.-B. Yang, X.-D. Fang, S.-J. Chen, Q.-Q. Xu, Q.-X. Li, A luminescent cadmium(ii) metal–organic framework based on a triazolate–carboxylate ligand exhibiting selective gas adsorption and guest-dependent photoluminescence properties, CrystEngComm 17 (2015) 4787–4792.
[47] N. Kajal, S. Gautam, Efficient nitro-aromatic sensor via highly luminescent Zn-based metal-organic frameworks, Chem. Eng. J. Adv. 11 (2022) 100348.